

June 4, 2018

Active Galactic Nuclei in the Sloan Digital Sky Survey: I. Sample Selection

Lei Hao^{1,2}, Michael A. Strauss¹, Christy A. Tremonti³, David J. Schlegel¹,
 Timothy M. Heckman⁴, Guinevere Kauffmann⁵, Michael R. Blanton⁶, Xiaohui Fan³,
 James E. Gunn¹, Patrick B. Hall¹, Željko Ivezić¹, Gillian R. Knapp¹, Julian H. Krolik⁴,
 Robert H. Lupton¹, Gordon T. Richards¹, Donald P. Schneider⁷, Iskra V. Strateva¹,
 Nadia L. Zakamska¹, J. Brinkmann⁸, Robert J. Brunner⁹, Gyula P. Szokoly⁵

ABSTRACT

We have compiled a large sample of low-redshift active galactic nuclei (AGN) identified via their emission line characteristics from the spectroscopic data of the Sloan Digital Sky Survey. Since emission lines are often contaminated by stellar absorption lines, we developed an objective and efficient method of subtracting the stellar continuum from every galaxy spectrum before making emission line measurements. The distribution of the measured H α Full Width at Half Maxima values of emission line galaxies is strongly bimodal, with two populations separated at about 1,200 km s⁻¹. This feature provides a natural separation between narrow-line and broad-line AGN. The narrow-line AGN are identified using standard emission line ratio diagnostic diagrams. 1,317 broad-line and 3,074 narrow-line AGN are identified from about 100,000 galaxy spectra selected over 1151 square degrees. This sample is used in a companion paper to determine the emission-line luminosity function of AGN.

Subject headings: galaxies: active — galaxies: Seyfert — galaxies: starburst — galaxies: quasars: emission lines — surveys

¹Princeton University Observatory, Princeton, NJ 08544

²Current address: Astronomy Department, Cornell University, Ithaca, NY 14853; hao1@isc.astro.cornell.edu

³Steward Observatory, University of Arizona, 933 North Cherry Avenue, Tucson, AZ 85721

⁴Department of Physics and Astronomy, Johns Hopkins University, 3400 North Charles Street, Baltimore, MD 21218

⁵Max-Planck Institut für Astrophysik, D-85748 Garching, Germany

⁶Center for Cosmology and Particle Physics, Department of Physics, New York University, 4 Washington Place, New York, NY 10003

⁷Department of Astronomy and Astrophysics, Pennsylvania State University, University Park, PA 16802

⁸Apache Point Observatory, P.O. Box 59, Sunspot, NM 88349-0059.

⁹Department of Astronomy and National Center for Supercomputer Applications, University of Illinois, 1002 West Green Street, Urbana, IL 61801.

1. Introduction

Ever since the definition of Seyfert galaxies (Seyfert 1943) and the first recognition of quasars (Schmidt 1963), astronomers have put enormous effort into compiling large samples of active galactic nuclei (AGN, in this paper, “AGN” refers to active galactic nuclei at all luminosities, including quasars) and trying to understand the physics that powers them. This is not easy, since luminous AGN comprise only a few percent of normal galaxies. Based on the distinctive characteristics of AGN, different methods have been developed to search for AGN in various wavebands.

In the optical, AGN show different colors from stars and normal galaxies, especially at high luminosity. Many surveys have used color selection (e.g. Schmidt & Green 1983; Boyle et al. 1990). In particular, the Sloan Digital Sky Survey (SDSS) (York et al. 2000) uses optical colors to identify quasar candidates, which are then observed spectroscopically (Richards et al. 2002). The color selection is very efficient but it requires that the optical luminosity of an AGN be at least comparable to the luminosity of its host galaxy for the color to be distinctive, and thus the color selection systematically misses less luminous AGN at low redshift.

AGN also show strong optical and ultraviolet emission lines. Broadly speaking, AGN can be classified into two types: broad-line and narrow-line AGN. The former show broad permitted emission lines, with Full Width at Half Maxima (FWHM) of several thousand km s^{-1} , while in narrow-line AGN, both the permitted and forbidden emission lines are narrow, with FWHMs $\sim 500 \text{ km s}^{-1}$. This is comparable with emission lines in normal star-forming galaxies, but emission lines in narrow-line AGN have considerably greater ionization range. In particular, both high-ionization lines such as $[\text{NeIII}]\lambda 3869$, $[\text{Ne V}]\lambda 3426$ and $[\text{OIII}]\lambda 5007$, and low-ionization lines such as $[\text{OI}]\lambda 6300$ and $[\text{NI}]\lambda 5200$, are stronger in narrow-line AGN than in normal starforming galaxies. Based on this feature, narrow-line AGN can be identified by their distinctive emission line ratios.

The first line ratio diagram was introduced by Baldwin, Phillips & Terlevich (1982), who suggested that AGN generically have greater $[\text{OIII}]\lambda 5007/\text{H}\beta$ (the flux ratio of $[\text{OIII}]\lambda 5007$ to $\text{H}\beta$) than do galaxies whose emission lines are due to stellar processes. Veilleux & Osterbrock (1987) developed their idea and used diagnostic diagrams that consist of combinations of four line ratios: $[\text{OIII}]\lambda 5007/\text{H}\beta$, $[\text{NII}]\lambda 6584/\text{H}\alpha$, $[\text{OI}]\lambda 6300/\text{H}\alpha$ and $[\text{SII}]\lambda\lambda 6716, 31/\text{H}\alpha$, and further developed a semi-empirical line on the diagrams to separate AGN and starburst galaxies. The emission-line pairs are chosen specifically so that the two lines in a ratio are at nearly identical wavelengths, therefore reddening and spectrophotometric uncertainties are not big effects. These diagnostic diagrams have been used ever since as a standard to identify narrow-line AGN.

Kewley et al. (2001) developed a set of theoretical separation lines for AGN and starforming galaxies on the diagnostic diagrams. By constructing a detailed continuous starburst model with large realistic metallicity and ionization parameter ranges, they found that the model folds on the diagnostic diagrams and there exist upper limits for starforming galaxies. These upper limits can be used to separate AGN and starforming galaxies and they can be fitted to a simple rectangular

hyperbolic shape:

$$\begin{aligned}
 \log\left(\frac{[\text{OIII}]\lambda 5007}{\text{H}\beta}\right) &= \frac{0.61}{\log([\text{NII}]/\text{H}\alpha) - 0.47} + 1.19 \\
 \log\left(\frac{[\text{OIII}]\lambda 5007}{\text{H}\beta}\right) &= \frac{0.72}{\log([\text{SII}]/\text{H}\alpha) - 0.32} + 1.30 \\
 \log\left(\frac{[\text{OIII}]\lambda 5007}{\text{H}\beta}\right) &= \frac{0.73}{\log([\text{OI}]/\text{H}\alpha) + 0.59} + 1.33
 \end{aligned}
 \tag{1}$$

These theoretical separation lines between AGN and starforming galaxies are widely accepted to use to identify narrow-line AGN in the diagnostic diagrams.

Kauffmann et al. (2003a), on the other hand, when studying host galaxy properties of narrow-line AGN in the SDSS, proposed an empirical and more lenient cut to identify AGN:

$$\log\left(\frac{[\text{OIII}]\lambda 5007}{\text{H}\beta}\right) \geq \frac{0.61}{\log([\text{NII}]/\text{H}\alpha) - 0.05} + 1.3
 \tag{2}$$

This criterion will select many more galaxies as AGN than Kewley’s criteria. In this paper, we apply both criteria and discuss their differences in detail.

There are several spectroscopic galaxy surveys from which people have tried to select AGN based on their emission lines. One is the CfA redshift survey (Davis, Huchra & Latham 1983; Huchra et al. 1983). Spectra of about 2,400 galaxies were taken to study their large scale distribution. Huchra, Wyatt & Davis (1982) used these spectra to select AGN by identifying emission lines indicative of nonstellar activity. As a result they found roughly 50 Seyfert galaxies, divided approximately equally between Seyfert 1 and Seyfert 2 galaxies, making the local Seyfert fraction $\sim 2\%$ (Huchra & Burg 1992).

Another example is the Revised Shapley-Ames catalog of bright galaxies (Sandage & Tammann 1981). Among its $\sim 1,300$ galaxies, about 50 are Seyfert galaxies of luminosity comparable to those found in the CfA Survey. Ho et al. (1997a) took uniform high signal to noise ratio (S/N) spectra of 486 galaxies using very small apertures centered on the nuclei. 418 galaxies were found to contain emission-line nuclei, of which 206 are star-forming, and 211 show AGN activity. This demonstrates that low-luminosity AGN activity in the local universe is extremely common, as first discussed by Phillips, Charles, & Baldwin (1983).

Hall et al. (2000) systematically selected high redshift AGN based either on their broad emission lines or narrow [NeV] emission lines from the Canadian Network for Observational Cosmology field galaxy redshift survey (CNOC2; Yee et al. 2000). They found 47 confirmed and 14 candidate AGN in the redshift range $0.27 \leq z \leq 4.67$.

The SDSS has opened a new window to the study of AGN by providing a huge number of high quality spectra of galaxies. There have been several studies identifying AGN spectroscopically from different subsamples of SDSS galaxies (Kauffmann et al. 2003a; Miller et al. 2003). Both studies

have focused on narrow-line AGN identified from the diagnostic diagrams. Miller et al. (2003) found AGN signatures in at least 20% of 4,921 galaxies in the redshift range $0.05 < z < 0.095$, and studied the environment of these AGN. Kauffmann et al. (2003a) selected 22,623 narrow-line AGN from a parent sample of 122,808 galaxies and studied their host galaxy properties. The AGN detection rate, however, depends very much on the AGN selection criteria used and many other details in defining the sample. In this paper, we apply a systematic search for both broad and narrow-line AGN in a well-defined sky area in the redshift range $0 < z < 0.33$. The framework of our narrow-line AGN selection is similar to Kauffmann et al. (2003a), but we differ in many details.

In section 2, we give a brief overview of the SDSS, focusing on those aspects most relevant to our study. §3 introduces the parent sample from which we will select our AGN. In §4, we will discuss the subtraction of stellar absorption lines from the spectra. The emission line measurements are discussed in §5. In §6, the selected AGN are presented and discussed. §7 gives a clean AGN sample and we summarize in §8.

2. The Sloan Digital Sky Survey

The Sloan Digital Sky Survey (York et al. 2000) is an imaging and spectroscopic survey that will eventually cover approximately one-quarter of the Celestial Sphere and collect spectra of $\sim 10^6$ galaxies and 10^5 quasars. It uses a dedicated 2.5m telescope at Apache Point, New Mexico, with a 3 degree field, and a mosaic CCD camera and two fiber-fed double spectrographs to carry out the imaging and spectroscopic surveys respectively. A separate 20" photometric telescope is used for photometric calibration (Smith et al. 2002; Hogg et al. 2001). The imaging camera (Gunn et al. 1998) consists of a mosaic of 30 imaging CCDs with $24 \mu\text{m}$ pixels subtending $0.396''$ on the sky. The sky is observed through five broad-band filters (u, g, r, i, z) (Fukugita et al. 1996; Stoughton et al. 2002) covering the entire optical band from the atmospheric cutoff in the blue to the sensitivity limit of silicon CCDs in the red. The imaging is done in drift-scan mode and the total integration time per filter is 54.1s. The 50% completeness limits for point sources are 22.5, 23.2, 22.6, 21.9 and 20.8 magnitudes respectively and the photometric calibration is reproducible to 3%, 2%, 2%, 2% and 3% for the five bandpasses, respectively. The image data are processed by a series of automated pipelines (Lupton et al. 2001; Stoughton et al. 2002; Pier et al. 2003), which make various measurements of the flux of each detected object.

The SDSS is obtaining spectra of complete samples of three categories of objects: Galaxies, Luminous Red Galaxies and Quasars. These spectroscopic targets are selected from the imaging data via various target selection criteria. Galaxy target selection is discussed in Strauss et al. (2002). Briefly speaking, galaxies are separated from stars by morphology. The magnitude limit cut for the galaxy sample was changed several times during commissioning, but is currently $r = 17.77$, where r represents the r band Petrosian magnitude. All magnitudes are corrected for extinction following Schlegel et al. (1998). These objects are the sample from which we will select AGN.

Quasar target selection (Richards et al. 2002) is based on the nonstellar colors of quasars and matching unresolved sources to the FIRST radio catalog. Luminous Red Galaxies are selected (Eisenstein et al. 2001) by a variant of the photometric redshift method, aiming to have a uniform, approximately volume-limited sample of highly luminous objects with the reddest colors in the rest frame to $z = 0.5$. In this paper, we will not discuss AGN selected from these two samples, unless they also satisfy the galaxy sample magnitude cut $r = 17.77$.

The SDSS spectra are taken with two fiber-fed spectrographs, covering the wavelength range 3800-9200 Å over 4098 pixels. Each plate can hold 640 fibers, with a fixed aperture of 3". The plates are positioned by a tiling algorithm (Blanton et al. 2003) and fibers are assigned to targets. Galaxies are among the tiled targets that have the highest priority of having their spectra taken. The finite diameter of the fiber cladding prevents fibers on any given plate from being placed closer than 55" apart. The resolution $\lambda/\Delta\lambda$ varies between 1850 and 2200. The relative spectrophotometry is accurate to about 20%. Each spectrum is accompanied by an estimated error per pixel, based on photon statistics and the amplitude of sky residuals. The typical S/N for galaxy spectra at the sample limit is 16/pixel.

The spectroscopic data are reduced through the spectroscopic pipelines, spectro2d and specBS. Spectro2d reduces the 2-dimensional spectrograms produced by the spectrographs to flux- and wavelength-calibrated spectra. SpecBS is different from the SDSS official pipeline, it determines classifications and redshifts via a χ^2 fit to the spectrum in question with a series of rest-frame star, galaxy and quasar templates. The basic technique is described by Glazebrook et al. (1998) and Bromley et al. (1998).

Even though specBS has made measurements on emission lines by fitting a single Gaussian at positions of each expected emission line, we carry out our own fits in our study. The main reason is that a single Gaussian fit is not adequate to model some AGN having both broad and narrow emission lines. The emission lines are measured directly from calibrated spectra, as we describe in detail in §5.

3. Parent Sample

In order to do statistical studies of AGN, it makes sense to start with a complete sample of objects within a certain well defined area from the SDSS. We start from 129,625 target objects complete in 1151 square degrees. This is about 1/2 of the spectra available in the SDSS Second Data Release (Abazajian et al. 2004). Among these objects, there are 98,684 galaxies targeted by the main galaxy target algorithm (Strauss et al. 2002; §2) and 17,972 quasar target objects (Richards et al. 2002; §2). In this paper, we will focus on the galaxy target objects. However, there are 2057 extragalactic objects selected as quasar targets with $r(\text{Petrosian}) \leq 17.77$, which were not targeted as galaxies because they are unresolved, and we include them in our galaxy sample. Among these 100,741 galaxies, most of them (99,990) have redshift $z < 0.33$, guaranteeing that the

H α emission line lies in our spectral coverage. H α is a very useful emission line in identifying AGN (Equation 2), and we limit our galaxy sample to these 99,990 objects.

4. Stellar Subtraction

AGN are identified by their emission line characteristics. As described in §2, the SDSS galaxy spectra are taken through a fixed 3'' aperture, which is large enough to let through not only the light from the nucleus but also substantial amounts of stellar light from the host galaxy. For example, at the median redshift of the sample ($z = 0.1$), a 3'' aperture subtends about $4h^{-1}$ kpc. Moreover, galaxies with higher redshift will have a larger host galaxy component in the observed spectra. Thus the nuclear emission lines are often contaminated by the stellar absorption lines of the host galaxy. For weak AGN, this contamination can be so severe that the interesting emission lines are completely submerged in the absorption lines. Thus before considering AGN selection, we have to develop a technique to properly remove the stellar absorption lines.

The basic idea of stellar subtraction is to build a library of stellar absorption line spectra templates, and use them as building blocks to simulate the stellar spectrum of the object in question. The library needs to be complete in the sense that it contains enough information on various absorption features to be able to simulate the stellar components of various galaxies with widely spread metallicities, ages and velocity dispersions. The library is typically composed of star spectra generated from a population synthesis code (Bica 1988; Saraiva et al. 2001, Kauffmann et al. 2003b) or direct observational spectra of absorption line galaxies (Ho et al. 1997a) or stars (Engelbracht et al. 1998). In this paper the library is constructed by applying the Principal Component Analysis (PCA) technique (e.g Connolly et al. 1995; Lahav et al. 1996; Bromley et al. 1998; Eisenstein et al. 2003; Yip et al. 2004) to a sample of pure absorption-line galaxies.

The advantages of building stellar absorption templates via this method are two-fold: only the first few eigenspectra are significant, so we can limit the size of the library without losing much useful information. Moreover, the eigenspectra are orthogonal to each other, resulting in a unique solution to the stellar subtraction fit using these templates.

4.1. Preparing the Absorption Line Galaxy Sample

We wish to identify a sample of pure absorption-line galaxies. In practice, we require that the H α equivalent width $EW(H\alpha) < 0$ (positive EW corresponds to emission lines), and that [OII] λ 3727 not be detected. [OII] λ 3727 is used because it is always apparent even in very weak emission line galaxies. Due to the presence of complex absorption near [OII] λ 3727, we measure this line after subtracting a preliminary PCA sample solely with the requirement that $EW(H\alpha) < 0$. A Gaussian function is fit to the residuals between $\lambda = 3700$ and $\lambda = 3754$. If the χ^2 of the fit is less than the χ^2 of a linear fit minus 3, the line is considered significant, and the object is rejected as an

absorption-line galaxy.

By limiting ourselves further to high S/N spectra, we defined three samples of several hundred pure absorption line galaxies grouped by their redshifts: 325 galaxies with $0.02 < z < 0.06$; 338 with $0.06 < z < 0.12$ and 372 with $0.12 < z < 0.22$. PCA is done on each group separately, giving three sets of eigenspectra that each can be used to subtract stellar components for galaxies of similar redshifts. We divide the sample in three groups in order to obtain a larger wavelength coverage for each group as well as the resultant eigenspectra. Figure 1 shows the mean of the spectra (i.e., the first eigenspectrum) in each galaxy group. They are essentially identical, although the lowest-redshift sample has slightly higher S/N.

The galaxies within the three groups are shifted to fixed rest-frame wavelength bins using sinc interpolation. Afterwards, each spectrum is normalized to a constant flux value. Unlike some PCA analyses (e.g., Eisenstein et al. 2003), the continua are not subtracted from the spectra before PCA. Each sample includes several hundred normalized galaxy spectra, which we express as a matrix S of dimensions $N \times M$, where N is the total number of galaxies in each group and M is the total number of common wavelength bins. Singular Value Decomposition (SVD) is used to build the eigenspectra (Connolly et al. 1995; Bromley et al. 1998).

4.2. PCA Result and Stellar Subtraction

The PCA analysis generates a set of eigenspectra, with main features of the absorption-line galaxies concentrated in the first few. In this study we will use the first eight eigenspectra as the stellar absorption-line templates. Empirical tests show that including more eigenspectra, which are basically just noise, does not improve the subtraction further. A χ^2 minimizing algorithm was adopted to determine the synthetic stellar absorption spectrum for each galaxy. The minimizing is done over the entire observed wavelength range except regions around the strongest emission lines found in AGN and starforming galaxies: $H\alpha$, $H\beta$, $[\text{NII}]\lambda\lambda 6548, 84$, $[\text{OIII}]\lambda 5007, \lambda 4959$ and $[\text{OII}]\lambda 3727$.

Since the stellar templates are eigenspectra of a sample of pure absorption line galaxies and galaxies having young stellar populations tend to have emission lines, the resultant eigenspectra mainly represent old stellar spectral features. Thus these eigenspectra are not representative of galaxies containing a young stellar component. One possible resolution would be to make sure that the PCA sample included enough E+A galaxies, which contain young stellar populations and do not have emission lines (Goto et al. 2003; Quintero et al. 2004). In this work, however, we simply add an A star spectrum selected from the SDSS spectroscopic data to the absorption-line template library to represent the young stellar population. Figure 2 shows an example of the stellar subtraction with and without this template, for a galaxy with a young star population. The improvement using the A star template is dramatic.

The stellar subtraction is automatically done to all galaxies in our parent galaxy sample,

including those quasars that satisfy the galaxy target selection magnitude cut (§ 2 and 3). However, doing stellar subtraction to a bright quasar dominated by a non-thermal continuum in the spectrum will certainly be a disaster. We thus add a pure power-law spectrum, written as $e_{\text{powerlaw}} \propto \lambda^{-1.5}$, to our template library. Figure 3 shows an example of stellar subtraction for a quasar with and without the power-law template. The power-law template significantly improves the subtraction. Since the spectrophotometry is not perfect, quasars have a range of intrinsic power-law slopes (Richards et al. 2002), and the power law fit can be systematically in error due to FeII emission (Figure 3 and Vanden Berk et al. 2001), the power-law template will certainly not be sufficient for clean continuum subtraction for all quasars. However we have found it to be adequate for our purposes. For galaxies that do not have a nonthermal power-law component, this template can help compensate for continuum shape errors due to errors in spectrophotometry and internal reddening.

In summary, our template library includes 8 PCA eigenspectra of pure absorption line galaxies, a power-law continuum and an A star spectrum. As demonstrated in Figures 2, 3 and further in Figure 4, weak emission lines such as $H\beta$ that were originally submerged in the stellar absorption line are successfully recovered. Moreover, emission lines such as $[\text{OI}]\lambda 6363$ and $[\text{NI}]\lambda 5200$ which are not apparent at all in the original spectrum clearly stand out after the subtraction. The subtraction also helps correct the strength of $H\alpha$, which is very important in subsequent AGN identification using emission line ratios.

The stellar subtraction is robust for galaxies of a range of velocity dispersions. Figure 4 shows two galaxies with very different velocity dispersions (Bernardi et al. 2003); note that in both cases, the subtracted spectrum shows no appreciable residuals of the strong absorption lines. The eigenspectra include terms that can give absorption lines of different width. This is another advantage of the PCA technique over the use of stellar libraries: we do not need to convolve each template with a Gaussian broadening function for each galaxy.

The whole procedure of doing PCA and stellar subtraction using the resultant eigenspectra is quite straightforward. Once the stellar component is subtracted, the emission lines can be measured, as we now describe.

5. Emission Line Measurements

Since we are mainly interested in emission-line galaxies, we will first set up a criterion to remove the pure absorption-line galaxies from the parent sample. We require that the EW of the $H\alpha$ line (in the rest frame) be greater than 3 \AA . In the rare cases in which the $H\alpha$ line is saturated or affected by bad pixels, we examine the equivalent width of the $[\text{OIII}]\lambda 5007$ and $H\beta$ lines, requiring that one of them be greater than 3 \AA . These equivalent widths are based on the line strength after stellar continuum subtraction, divided by the stellar continuum itself.

This criterion also rejects weak emission line galaxies. This is acceptable since the S/N ratio for these lines will be low and thus our ability to distinguish AGN from starbursts will be poor. A

total of 42,435 galaxies, about half of the parent galaxy sample, pass the equivalent width cut. We refer to this sample as the emission line galaxy sample. All AGN are selected from this sample.

The intensity, full width at half maximum (FWHM), central wavelength and nearby continuum value of the main emission lines in these galaxies are measured via Gaussian fits weighted by the estimated errors per pixel. The following emission lines are needed for AGN selection: $\text{H}\alpha$, $[\text{NII}]\lambda 6584$, $\text{H}\beta$, $[\text{OIII}]\lambda 5007$, $[\text{SII}]\lambda 6716$, 31 and $[\text{OI}]\lambda 6300$. The following lines are fit with a single Gaussian: $\text{H}\beta$, $[\text{OIII}]\lambda 5007$ and $[\text{OI}]\lambda 6300$. The $[\text{SII}]$ doublet is fit with a two-Gaussian function model. The FWHMs and intensities of the two Gaussians are independent of each other, while the central wavelengths are correlated with a single variable z , and the continuum is shared by the two Gaussian functions. Since our fitting is done to a stellar continuum subtracted spectrum that has been shifted to rest wavelength, the fitting results for z and the continuum are very close to zero. The $\text{H}\alpha$ and $[\text{NII}]\lambda 6548$, 84 lines are fitted with three Gaussians. The FWHMs of the $[\text{NII}]$ lines are kept the same and the intensity ratio of $[\text{NII}]\lambda 6584$ to $[\text{NII}]\lambda 6548$ is fixed to 3, as required by the energy level structure of the $[\text{NII}]$ ion (Osterbrock 1989). Again, the central wavelengths of $\text{H}\alpha$ and the $[\text{NII}]$ doublet are correlated with a single redshift parameter and the three lines share the same continuum value. The pixels located within 100 \AA of the central wavelength of the emission lines are used for Gaussian fits (adjacent emission lines in this range are shielded out). However, in order to be sensitive to a broad component of $\text{H}\alpha$, we fit the $\text{H}\alpha$, $[\text{NII}]$ group to the range $6565 \text{ \AA} \pm 300 \text{ \AA}$ (the adjacent $[\text{OI}]$ and $[\text{SII}]$ lines are masked in the fit). We will use the χ^2 of the fit to test for the significance of the broad component, restricting ourselves to the range $6565 \text{ \AA} \pm 80 \text{ \AA}$ to reduce the sensitivity to uncertainties in the continuum.

Some AGN show both broad and narrow permitted emission lines. For these galaxies, a single Gaussian function for $\text{H}\alpha$ is obviously not appropriate. To take this into account, we also fit the $\text{H}\alpha$ and $[\text{NII}]$ doublet with a four-Gaussian model: two for the $[\text{NII}]$ lines and two for $\text{H}\alpha$. The two $\text{H}\alpha$ Gaussian functions have the same central wavelength, but different intensities and FWHMs. The final decision of which model (the three-Gaussian model or the four-Gaussian model) to use for a given galaxy is done by comparing the χ^2 of the two model fits, χ_3^2 and χ_4^2 respectively. In particular, we choose the four-Gaussian model fit when:

$$(\chi_3^2 - \chi_4^2 - 2)/\chi_4^2 > 0.2 \quad (3)$$

This criterion is empirical, but is inspired by a similar statistic for linear fitting models (Lupton 1993). If we would like to fit a data set (x_i, y_i) with a linear fitting model $y_{\text{model}} = y(x)$, and the errors σ_i are Gaussian, then

$$\chi^2 = \sum_i \left(\frac{y_i - y_{\text{model}}}{\sigma_i} \right)^2 \quad (4)$$

follows a χ_{n-k}^2 distribution, where n and k are the numbers of the data points and the parameters used in the model respectively. If there are two linear models M and N , with k and $(k - r)$ parameters respectively (i.e. model M has r extra parameters), their χ^2 functions χ_N^2 , χ_M^2 will then follow χ_{n-k}^2 and $\chi_{n-(k-r)}^2$ distributions. It can be proved that for linear models, χ_M^2 and

$\chi_M^2 - \chi_N^2$ are independent, thus the quantity

$$f \equiv \frac{(\chi_N^2 - \chi_M^2)/r}{\chi_M^2/(n - k)} \quad (5)$$

follows a $F_{r, n-k}$ distribution. If f is large, then we can accept the hypothesis that the added parameters significantly improve the fit.

In our case, our models are non-linear in the parameters, and χ_M^2 and $\chi_M^2 - \chi_N^2$ will not be independent. The four-Gaussian model has two more degrees of freedom than does the three-Gaussian model, so the numerator of the criterion is written as $(\chi_3^2 - \chi_4^2 - 2)$. The limit “0.2” in equation (3) is an empirical number and is demonstrated to be appropriate from our manual inspection.

However it is not always unambiguous to identify the broad H α component using the above criterion, since not all emission lines are well-fit with Gaussians (Strateva et al. 2003). In particular, narrow emission lines generally have extended wings at their bases (Ho et al. 1997b). If the narrow emission line is strong, this non-Gaussian feature will become prominent, and a 4-Gaussian model will be chosen by Equation 3. In this case, the height of the broader component h_1 will be small compared to the height of the narrow component, h_2 and the Gaussian width of the broader component σ will be relatively small. To not count such cases as broad line, we stick with the 3-Gaussian fit for those objects which satisfy,

$$\sigma < 20 \text{ \AA} (\sim 2200 \text{ km s}^{-1}) \quad \text{and} \quad h_1/h_2 < 0.1 \quad (6)$$

no matter what the criterion of equation (3) might indicate.

We compared our empirical criterion (equation (6)) with the well defined Bayesian Information Criterion (BIC, Liddle 2004). We found that we are as efficient in choosing broad-line component as BIC, and at the same time, our criterion identifies far fewer fake broad-line components than BIC does.

After fitting all relevant emission lines, the line strengths are calculated based on the line fitting parameters. The observed SDSS spectra are accompanied by an estimated error per pixel, based on photon and read noise statistics and variation among sky spectra. These errors are approximately independent between pixels and are good to 8% (McDonald et al. 2004). In stellar continuum subtraction we assumed the stellar templates perfect since they are very high S/N. The errors in the line strengths are calculated using standard propagation of errors. Those emission lines that are less than 3σ detections are marked as weak. If they are needed in identifying an AGN, special care should be applied (§6.2).

6. AGN Statistics

6.1. Broad-Line AGN

The measured emission line parameters can be used to identify AGN from the emission line galaxy sample. We select broad-line AGN by checking the $H\alpha$ line width. Figure 5 gives the distribution of the FWHM values of the $H\alpha$ emission line for over 40,000 emission line galaxies. For galaxies that prefer two Gaussian components for $H\alpha$ (§5), the width of the broader component is plotted. The distribution is clearly bimodal, with a minimum at $1,200 \text{ km s}^{-1}$. The first peak is at about 200 km s^{-1} , which reflects the resolution limit of the SDSS spectrographs. It extends far above the limit of the plot, demonstrating that most of the galaxies in the sample are starforming galaxies with narrow $H\alpha$ lines. Clearly separated from these normal galaxies, the second group of galaxies has substantially larger $H\alpha$ FWHM value. Naturally, we use $\text{FWHM}(H\alpha) > 1,200 \text{ km s}^{-1}$ as the selection criterion for defining broad-line AGN.

The inserted plot in Figure 5 shows the $H\alpha$ FWHM distribution for AGN only (the detailed selection of narrow-line AGN is described in §6.2). Narrow-line AGN have typical $H\alpha$ FWHM values similar to those of usual emission-line galaxies. The paucity of objects with $\text{FWHM} \sim 1,200 \text{ km s}^{-1}$ is not well understood and will need to be explained in AGN unification models.

However, we should make sure that the bimodality is not a consequence of our fitting procedure in choosing the 4-Gaussian fitting model over the 3-Gaussian model. To do so, we intentionally change the limiting numbers of the criteria described in §5. We write the criteria (equations (3) and (6)) as:

$$(\chi_3^2 - \chi_4^2 - 2)/\chi_4^2 > A \quad \text{and} \quad (\sigma \geq B \quad \text{or} \quad h_1/h_2 \geq C) \quad (7)$$

Our default values are $A = 0.2$, $B = 20 \text{ \AA}$ (2182 km s^{-1}), $C = 0.1$. Now we change this set of numbers to $A = 0.6$, $B = 30 \text{ \AA}$ (3249 km s^{-1}), $C = 0.7$ separately. The changes will all reduce the number of objects with broad $H\alpha$ components. However, those galaxies which are distinctively broad will still be selected by the new criteria. The top two panels of Figure 6 shows the $H\alpha$ FWHM distribution with the changed criteria. As can be seen, no matter how the criteria are changed, the bimodality feature and the minimum at about $1,200 \text{ km s}^{-1}$ remain the same even though the number of selected broad-line AGN changes substantially. A complementary test is to loosen the criteria a little. Out of the concern that the $B = 20 \text{ \AA}$ cut might artificially reject objects with FWHM around $1,200 \text{ km s}^{-1}$, we change this criterion to $B = 0 \text{ \AA}$. The bottom panel of Figure 6 shows the $H\alpha$ FWHM distribution with $A = 0.2$, $B = 0 \text{ \AA}$ and $C = 0, 0.1, 0.7$ respectively. This yields many false broad-line AGN. However, the bimodality and the location of the minimum are still the same. Therefore, the bimodal feature is insensitive to the specific details of the criteria in equation (7).

One might also suspect that the bimodality is caused by the fact that the values we have used in the plot are coming from two different fitting models. In the distribution plot, the values of the narrower group usually come from the fitting parameters of the 3-Gaussian model while those of

the broader group are mostly from the 4-Gaussian model. The change from one model to another might cause some discontinuity in an otherwise continuous distribution. To test this, Figure 7 shows the distribution of width using the 3-Gaussian model fits alone; the bimodal feature is still apparent.

As a final check of the reality of the deficit of galaxies with $\text{FWHM} \sim 1,200 \text{ km s}^{-1}$, we carried out simulations of galaxies with composite $\text{H}\alpha$ profiles, in which the broad component had $1200 \text{ km s}^{-1} \leq \text{FWHM} \leq 2200 \text{ km s}^{-1}$ and $0.1 \leq h_1/h_2 \leq 0.3$, and to which we add a stellar continuum and characteristic noise. After putting these objects through our code, we found that we would miss only a small fraction of broad-line AGN with $\text{H}\alpha$ FWHM close to $1,200 \text{ km s}^{-1}$, not nearly enough to explain the bimodality. Therefore, the bimodal feature is clearly real.

Defining broad-line AGN as objects with $\text{H}\alpha$ FWHM $> 1,200 \text{ km s}^{-1}$, 1317 broad-line AGN are identified from 42,435 emission line galaxies. For those galaxies that need two $\text{H}\alpha$ Gaussian functions but are not classified as broad ($\text{FWHM}(\text{H}\alpha) < 1,200 \text{ km s}^{-1}$), we use a 3-Gaussian fit for $\text{H}\alpha$ and [NII] so that we can have consistent $\text{H}\alpha$ measurements when they are used in emission line ratio diagnostic diagrams, as we now describe.

6.2. Narrow-Line AGN

Narrow-line AGN cannot be separated cleanly from star-forming galaxies by their emission line widths. Therefore, we will use the traditional emission line ratio diagnostic diagrams (Veilleux & Osterbrock 1987; Section 1) to select them. In Figure 8 we place the galaxies in the emission line galaxy sample in these diagrams (broad-line AGN selected in Section 6.1 are excluded). Galaxies with relevant emission lines detected with less than 3σ significance are omitted in the diagrams. There are roughly 40,000 galaxies contained in the [NII]/ $\text{H}\alpha$ and [SII]/ $\text{H}\alpha$ diagrams, but only about 23,000 galaxies in the [OI]/ $\text{H}\alpha$ diagram. Due to the large number of galaxies available, we can see a continuous distribution in the diagrams. AGN have larger [OIII]/ $\text{H}\beta$, [NII]/ $\text{H}\alpha$, [OI]/ $\text{H}\alpha$ and [SII]/ $\text{H}\alpha$ values than do starbursts, and are clearly separated from the loci formed by starforming galaxies. The AGN and starforming galaxy separation lines developed by Kauffmann et al. (2003a, short-dashed), Kewley et al. (2001, solid) and Veilleux & Osterbrock (1987, dash-dot) are plotted in the diagram. Kauffmann’s and Kewley’s criteria agree much better with the shape of the density profile; the disagreement between Kewley’s lines and the data are almost all in the $\pm 0.1 \text{ dex}$ error range (dashed lines).

Within Kewley’s separation scheme, we can identify AGN as those located to the upper right of the lines. About 10% of all emission line galaxies are classified differently in the three diagrams. We will refer to these as mismatched galaxies. One half of these are classified as AGN by the [OI]/ $\text{H}\alpha$ diagram, but not by the other two. The same discrepancy was also noticed by Stasińska & Leitherer (1996) and Dopita et al. (2000), who ascribed the enhancement of [OI] lines in starburst galaxies to the mechanical energy released into the gas by supernovae and stellar winds. Dopita (1997)

noted that when even a weak shock compresses the gas, the postshock local ionization is sharply lowered, leading to a strong enhancement of the [OI] lines. Another quarter of the mismatched galaxies are those classified as AGN in the [SII]/H α diagram but not in the [NII]/H α diagram, and the [OI] line is of too low significance to use the [OI]/H α diagram. The cause could again be shock excitation: the relatively cool high-density regions formed behind the shock front emit strong [SII] emission lines (Dopita et al. 2000). The remaining quarter of the mismatched galaxies are randomly distributed, possibly due to noise. Overall, about 95% of the mismatched objects have enhanced [OI] or [SII] emission lines compared to the [NII] lines, perhaps due to shock excitation from supernovae and stellar winds in a starburst galaxy. The small overall number of mismatches demonstrates that Kewley’s theoretical separation lines give very consistent excitation mechanism classifications among the three diagrams.

Using Kewley’s scheme, we define the galaxies located to the upper right of the lines in all three diagrams as narrow-line AGN. If the emission lines used in the diagrams are weak (§5), we take special care: if the [NII] or [OIII] line is found to be weak, the galaxy will not be identified as an AGN unless the H α line is also broad. However, if the [OI] line or [SII] line is found to be weak, then the classification based on the [OI]/H α or [SII]/H α diagram is defined to be inconclusive and the identification of the galaxy depends on the remaining diagrams. Galaxies with one or two inconclusive classifications and AGN classifications in the remaining diagram(s) are also included in our sample. We do not include any mismatched objects in the final narrow-line AGN sample. Based on these criteria, 3074 narrow-line AGN are selected.

The selection criteria are different from those used by Kauffmann et al. (2003a) (Equation 2, Figure 8 short-dashed line). In the [NII]/H α vs. [OIII]/H β diagram, galaxies are distributed on two arms. Normal galaxies have weaker [NII]/H α ratio than do AGN. So it is expected that they form the locus on the left arm (with smaller [NII]/H α values) and galaxies on the right arm are AGN. But Kewley’s line cuts through the right arm. Kauffmann et al. propose to classify all galaxies located on the right arm as AGN, generating an empirical line separating the two branches. This line lies well below Kewley’s criterion in the [NII]/H α diagram and the number of galaxies which fall between the two criteria is very large.

This difference between the two criteria will cause tremendous disagreement on AGN statistics. If Kauffmann’s criterion is adopted, we would have selected about 10,700 narrow-line AGN, roughly three times the AGN selected via Kewley’s criterion. To understand the disagreement better, we divide the galaxies in the right arm into several groups by their locations along the arm; each group is assigned a different color in Figure 9. These galaxies are accordingly plotted in the [OI]/H α and [SII]/H α vs. [OIII]/H β diagrams. In addition, we plot the H α FWHM distribution for the galaxies in each group. Very interestingly, galaxies in the right arm form a similar sequence in the three diagrams: galaxies with larger [NII]/H α values usually have larger [OI]/H α and [SII]/H α values. Furthermore, galaxies with larger [NII]/H α or [OIII]/H β values typically have broader H α emission lines. This gives us a hint that some galaxies on the right arm might be galaxies with mixed AGN and starburst components, with a larger AGN component corresponding to a higher

position on the diagrams (Kauffmann et al. 2003a). However, some of the AGN and starburst composite galaxies are degenerate with starforming galaxies with widely spread metallicity and ionization parameters, especially in the $[\text{OI}]/\text{H}\alpha$ and $[\text{SII}]/\text{H}\alpha$ vs. $[\text{OIII}]/\text{H}\beta$ diagrams. Because of the degeneracy, Kewley’s separation lines, which are the upper limit for pure starburst galaxies, are unable to identify every galaxy with an AGN contribution.

Therefore, the AGN sample created using Kauffmann’s criterion includes these AGN + starburst composite galaxies; they make up the majority of the sample. While these galaxies include an appreciable contamination from star formation in their emission line strengths, the star formation contribution to $[\text{OIII}]$ is relatively weak (Kauffmann et al. 2003a). The AGN sample created using Kewley’s criterion includes only those that are unambiguously AGN dominated. Both samples have their pros and cons, so we will keep both samples. In Hao et al. (2005; paper II), the luminosity functions are measured for both samples and the results are compared.

Some of the narrow-line AGN have very strong low ionization lines; these objects are “Low Ionization Nuclear Emission Line Regions” (“LINERs”). Ever since the first definition of the LINER class by Heckman (1980), the excitation mechanism causing LINERs has remained unknown. There is vigorous debate on whether or not LINERs belong to the AGN family. Filippenko et al. (1985) showed that many LINERs have a broad emission-line component, suggesting they are indeed AGN. Kewley et al. (2001) established a series of starburst models and developed a set of extreme mixing lines, below which the galaxies can only be modeled by pure shocks without an ionizing precursor, or a power-law ionizing radiation field with an extremely low ionization parameter. The long-dashed lines in Figure 8 show the extreme mixing line in the $[\text{OI}]/\text{H}\alpha$ diagram. If this line alone is adopted here in selecting LINERs, there are 650 LINERs identified in the narrow-line AGN sample. These objects will be studied in detail in future work and will not be discussed further here.

It is interesting to know how the narrow components of broad-line AGN are located on the diagrams. In Figure 10, we select those broad-line AGN with real narrow $\text{H}\alpha$ components (whose line widths are less than 5 \AA) and plot their emission line ratio with the narrow components of $\text{H}\alpha$ and $\text{H}\beta$ in the diagram. Most of the broad-line AGN are concentrated on the right arm of the $[\text{NII}]/\text{H}\alpha$ vs. $[\text{OIII}]/\text{H}\beta$ diagram, indicating a strong AGN contribution. Therefore, the classifications of these galaxies from the narrow component and the broad component are consistent. There are also some broad-line AGN with their narrow components corresponding to locations to the right of the mixing line in the $[\text{OI}]/\text{H}\alpha$ diagram (Figure 8), these can be characterized as LINERs (Filippenko et al. 1985).

The final AGN sample includes 1,317 broad-line AGN, 3,074 narrow-line AGN if Kewley’s criteria are adopted and 10,700 narrow-line AGN with Kauffmann’s criteria. This AGN sample is complete over 1151 square degrees, defined by the criteria described in this paper¹⁰.

¹⁰The sample is available at: <http://isc.astro.cornell.edu/~haol/agn/agncatalogue.txt>

7. Summary

The large number of high quality spectra available in the SDSS provides us with great opportunities for AGN studies. In this paper, we have systematically identified AGN from the SDSS spectroscopic data from their emission line characteristics. In order to make unbiased measurements of the emission lines, we have carefully subtracted absorption stellar spectra from the observed spectra. The absorption line templates are constructed by applying PCA to pure absorption line galaxies. Emission lines are measured from corrected emission line spectra by fitting Gaussian functions. In particular, to obtain proper identification of broad emission lines, the H α and [NII] emission lines are fitted with both a three-Gaussian model and a four-Gaussian model. The final decision of which model to use is based on a comparison of χ^2 values of the two model fits.

Using measured parameters of the H α emission lines, broad-line AGN are identified. It is found that the distribution of H α FWHM values of emission-line galaxies in the parent sample is bimodal, with two populations separated at about 1,200km s $^{-1}$. Various tests have been applied to confirm that this feature is not caused by selection effects. The bimodal feature also gives a natural separation between broad-line and narrow-line AGN, and is significant in understanding the “unified theory” of AGN. A naive explanation could be that the physical parameters of the torus are correlated with the black hole mass. For an AGN with a black hole mass less than a certain value, the dust torus becomes so large that it almost totally blocks the broad-line region. Therefore, it is hard to observe any broad-line component with small H α FWHM values.

Narrow-line AGN are identified using traditional diagnostic diagrams. Due to the large number of galaxies available, starforming galaxies follow well-defined loci. Theoretical separation lines between AGN and starforming galaxies developed by Kewley et al. (2001) agree fairly well with the shape of the galaxy density contour and bring few mismatched classifications among the three diagrams. Only in the [NII]/H α diagram does Kewley’s line seem to disagree with the data, where the galaxies are distributed into two arms and Kewley’s line cuts through the right arm (larger [NII]/H α value). Kauffmann et al. (2003a) argued that all objects in the right arm should be considered as AGN. Based on the SDSS data, they proposed to use the empirical line separating the two arms to select AGN. This line is lower than Kewley’s line, and would classify many more objects than Kewley’s criterion as narrow-line AGN. We demonstrated that AGN selected via Kewley’s criterion only include those that are dominated by active nuclear activity, while AGN selected via Kauffmann’s criterion also includes AGN + starburst composite galaxies. Both samples have their pros and cons, and we keep both for further studies.

The final AGN sample, complete to magnitude cut $r(\text{Petrosian}) < 17.77$, includes 1317 broad-line and 3074 narrow-line AGN (10,700 if Kauffmann’s criterion is used) over 1151 square degrees. This is based on 1/8 the eventual SDSS survey; the sample will grow substantially. This sample is very useful for various studies. First, with the large number of AGN in this sample, we can evaluate the AGN luminosity functions; we carry out this analysis in Paper II. Second, by correlating these AGN with their host galaxy parameters, we can study the relationship between AGN and their

host galaxies for both narrow-line (Kauffmann et al. 2003a) and broad-line AGN. Third, from the velocity dispersion of the AGN host galaxies, we can directly measure the approximate black hole mass using the $M_{\text{BH}} - \sigma$ relation developed first in quiescent galaxies (Gebhardt et al. 2000; Ferrarese & Merritt 2000; Ferrarese et al. 2001; Tremaine et al. 2002), and further derive the accretion rate for various types of AGN (Heckman et al. 2004). This will help us to understand their accretion mechanisms. Fourth, we can measure the cluster properties and local environments of different types of AGN in the sample (Miller et al. 2003), which is important to constrain AGN formation scenario. Furthermore, we can also correlate this AGN sample with surveys in other wavebands, such as X-ray, radio, infrared, etc. to better understand the physics of AGN. Studies on these topics will be covered in future papers.

Acknowledgments. We would like to thank Lisa Kewley for useful discussions and comments.

Funding for the creation and distribution of the SDSS Archive has been provided by the Alfred P. Sloan Foundation, the Participating Institutions, the National Aeronautics and Space Administration, the National Science Foundation, the U.S. Department of Energy, the Japanese Monbukagakusho, and the Max Planck Society. The SDSS Web site is <http://www.sdss.org/>.

The SDSS is managed by the Astrophysical Research Consortium (ARC) for the Participating Institutions. The Participating Institutions are The University of Chicago, Fermilab, the Institute for Advanced Study, the Japan Participation Group, The Johns Hopkins University, the Korean Scientist Group, Los Alamos National Laboratory, the Max-Planck-Institute for Astronomy (MPIA), the Max-Planck-Institute for Astrophysics (MPA), New Mexico State University, University of Pittsburgh, Princeton University, the United States Naval Observatory, and the University of Washington.

L.H. and M.A.S. are supported in part by NSF grant AST-0071091 and AST-0307409. L.H. acknowledges the support of the Princeton University Research Board.

REFERENCES

- Abazajian, K. et al. , 2004, 128, 502
- Baldwin, J. A., Phillips, M. M., & Terlevich, R. 1981, *PASP*, 93, 5
- Bernardi, M., et al. 2003, *AJ*, 125, 1817
- Bica E. 1988, *A&A*, 192, 98
- Blanton, M. R., et al. 2003, *AJ*, 125, 2276
- Boyle, B. J., Fong, R., Shanks, R., & Peterson, B. A. 1990, *MNRAS*, 243, 1
- Bromley, B. C., Press, W. H., Lin, H., & Kirshner, R. P. 1998, *ApJ*, 505, 25
- Connolly, A. J., Szalay, A. S., Bershad, M. A., Kinney, A. L., & Calzetti, D. 1995, *AJ*, 110, 1071
- Davis, M., Huchra, J., Latham, D. 1983, *IAUS*, 104, 167
- Dopita, M. A. 1997, *ApJ*, 485, L41
- Dopita, M. A., Kewley, L. J., Heisler, C. A., Sutherland, R. S. 2000, *ApJ*, 542, 224
- Eisenstein, D. J., et al. 2001, *AJ*, 122, 2267
- Eisenstein, D. J., et al. 2003, *ApJ*, 585, 694
- Engelbracht, C. W., Rieke, M. J., Rieke, G. H., Kelly, D. M., Achtermann, J. M. 1998, *ApJ*, 505, 639
- Ferrarese, L., & Merritt, D. 2000, *ApJ*, 539, L9
- Ferrarese, L. et al. 2001, *ApJ*, 555, L79
- Filippenko, A. V., 1985, *ApJ*, 289, 475
- Fukugita, M., Ichikawa, T., Gunn, J. E., Doi, M., Shimasaku, K., & Schneider, D. P. 1996, *AJ*, 111, 1748
- Gebhardt, K. et al. 2000, *ApJ*, 539, L13
- Glazebrook, K., Offer, A. R., Deeley, K. 1998, *ApJ*, 492, 98
- Goto, T., et al. 2003, *PASJ*, 55, 771
- Gunn, J. E., et al. 1998, *AJ*, 116, 3040
- Hall, P. B., et al. 2000, *AJ*, 120, 2220
- Hao, L., et al. 2005, in preparation, (Paper II)
- Heckman, T. M. 1980, *A&A*, 87, 152
- Heckman, T. M., Kauffmann, G., Brinchmann, J., Charlot, S., Tremonti, C., White, S. D. M. 2004, *ApJ*, 613, 109
- Ho, L. C., Filippenko, A. V., & Sargent, W. L. W. 1997a, *ApJS*, 112, 315
- Ho, L. C., Filippenko, A. V., Sargent, W. L. W., & Peng, C. Y. 1997b, *ApJS*, 112, 391

- Hogg, D. W., Finkbeiner, D. P., Schlegel, D. J., Gunn, J. E., 2001, *AJ*, 122, 2129
- Huchra, J., Davis, M., Latham, D., Tonry, J. 1983, *ApJS*, 52, 89
- Huchra, J., Burg, R. 1992, *ApJ*, 393, 90
- Huchra, J. P., Wyatt, W. F., Davis, M. 1982, *AJ*, 87, 1628
- Kauffmann, G., et al. 2003a, *MNRAS*, 346, 1055
- Kauffmann, G., et al. 2003b, *MNRAS*, 341, 33
- Kewley, L. J., Dopita, M. A., Sutherland, R. S., Heisler, C. A., Trevena, J. 2001, *ApJ*, 556, 121
- Lahav, O., Naim, A., Sodr e, L., Jr., Storrie-Lombardi, M. C. 1996, *MNRAS*, 283, 207
- Liddle, A. R. 2004, *MNRAS*, 351, L49
- Lupton, R. H. 1993, *Statistics in Theory and Practice* (Princeton University Press)
- Lupton, R. H., Gunn, J. E., Ivezi c, Z., Knapp, G. R., Kent, S., & Yasuda, N. 2001, in *ASP Conf. Ser. 238, Astronomical Data Analysis Software and Systems X* (San Francisco: ASP), 269
- McDonald, P., et al. 2004, *astro-ph/0405013*
- Miller, C. J., Nichol, R. C.; G omez, P. L., Hopkins, A. M. & Bernardi, M. *ApJ*, 2003, 597, 142
- Osterbrock D. E. 1989, *Astrophysics of Gaseous Nebulae and Active Galactic Nuclei* (Mill Valley: Univ. Science Books)
- Phillips, M. M., Charles, P. A., Baldwin, J. A. 1983, *ApJ*, 266, 485
- Pier, J. R., et al. 2003, *AJ*, 125, 1559
- Quintero, A. D., et al. , 2004, *ApJ*, 602, 190
- Richards, G. T., et al. 2002, *AJ*, 123, 2945
- Saraiva, M. F., Bica, E., Pastoriza, M. G., & Bonatto, C. 2001, *A&A*, 376, 43
- Sandage, A., & Tammann, G. 1981, *A Revised Shapley-Ames Catalog of Bright Galaxies* (Carnegie Inst. Washington Pub. 635)
- Schlegel, D. J., Finkbeiner, D. P., Davis, M. 1998, *ApJ*, 500, 525
- Schmidt, M. 1963, *Nature*, 197, 1040
- Schmidt, M., & Green, R. F. 1983, *ApJ*, 269, 352
- Seyfert, C. K. 1943, *ApJ*, 97, 28
- Smith, J. A., et al. 2002, *AJ*, 123, 2121
- Stasi nska, G., & Leitherer, C. 1996, *ApJS*, 107, 661
- Stoughton, C., et al. 2002, *AJ*, 123, 485
- Strateva, I., et al. 2003, *AJ*, 126, 1720
- Strauss, M. A., et al. 2002, *AJ*, 124, 1810

- Tremaine, S., et al. , 2002, ApJ, 574, 740
Vanden Berk, D. E., et al. 2001, AJ, 122, 549
Veilleux, S., & Osterbrock, D. E. 1987, ApJS, 63, 295
Yee, H. K. C., et al. 2000, ApJS, 129, 475
Yip, C. W., et al. 2004, AJ, 128, 585
York, D. G. et al. 2000, AJ, 120, 1579

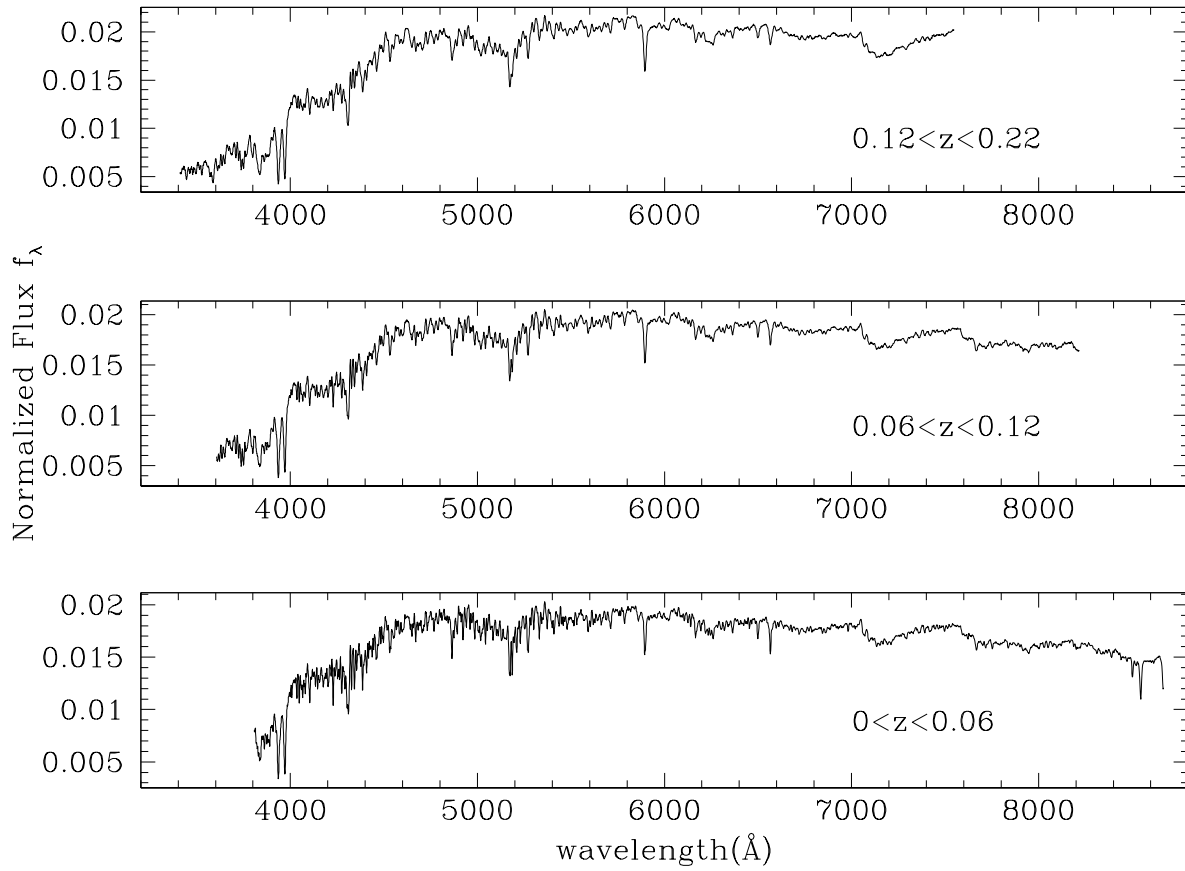


Fig. 1.— The mean spectra of pure absorption-line galaxies in three groups of redshift. Within the common wavelength range, the mean spectra are almost identical, although the S/N is highest at lowest redshift. PCA is applied to each group and three sets of eigenspectra are obtained.

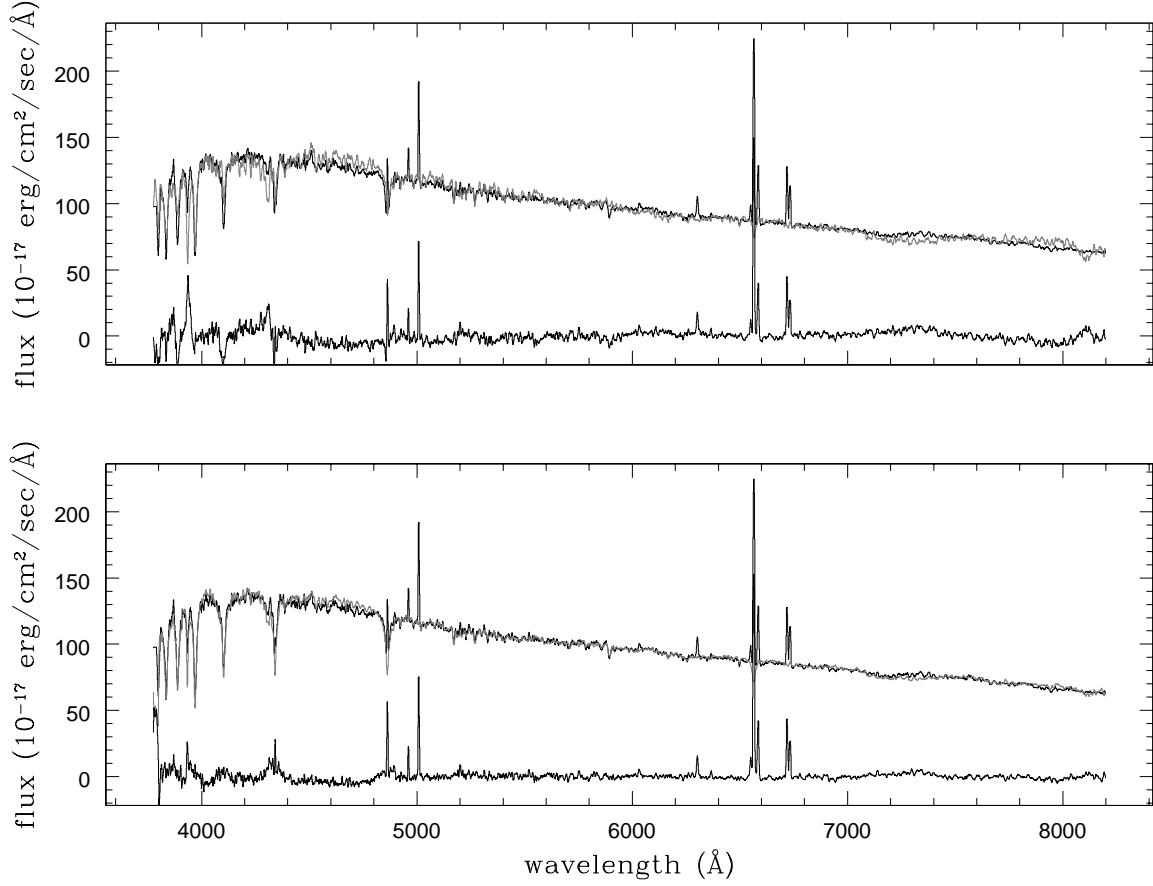


Fig. 2.— A subtraction example (a normal starforming galaxy) comparing stellar-subtraction without (top) and with (bottom) an A star spectrum included among the absorption-line templates. The grey spectra are the stellar spectra constructed using the absorption-line templates. The A star spectrum significantly improves the performance of the stellar subtraction in this case. Note that the subtraction makes weak emission lines such as [OI] λ 6363 more prominent.

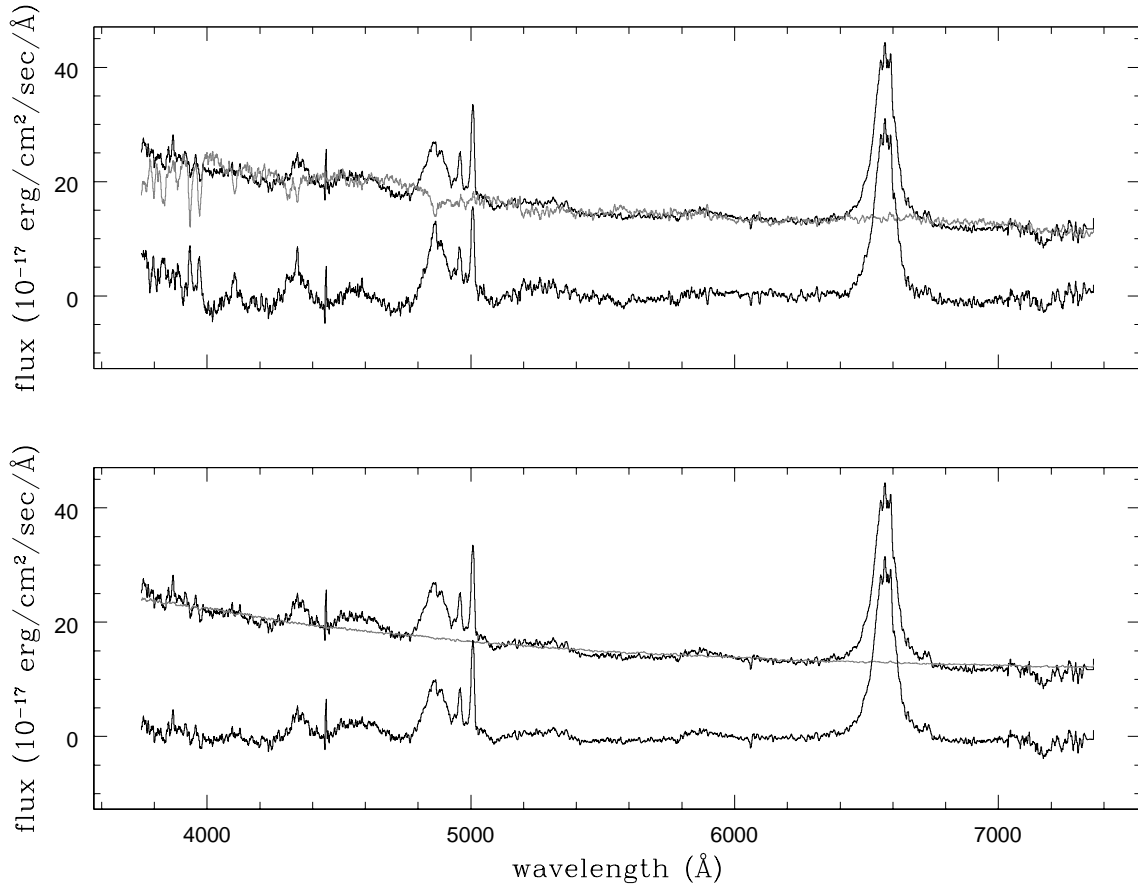


Fig. 3.— A subtraction example comparing stellar-subtraction without (top) and with (bottom) a power-law spectrum included in the absorption-line templates. The power-law spectrum helps to properly subtract the quasar continuum without generating fake emission lines. Note the presence of FeII $\lambda 4570$ here, which does affect the continuum fit.

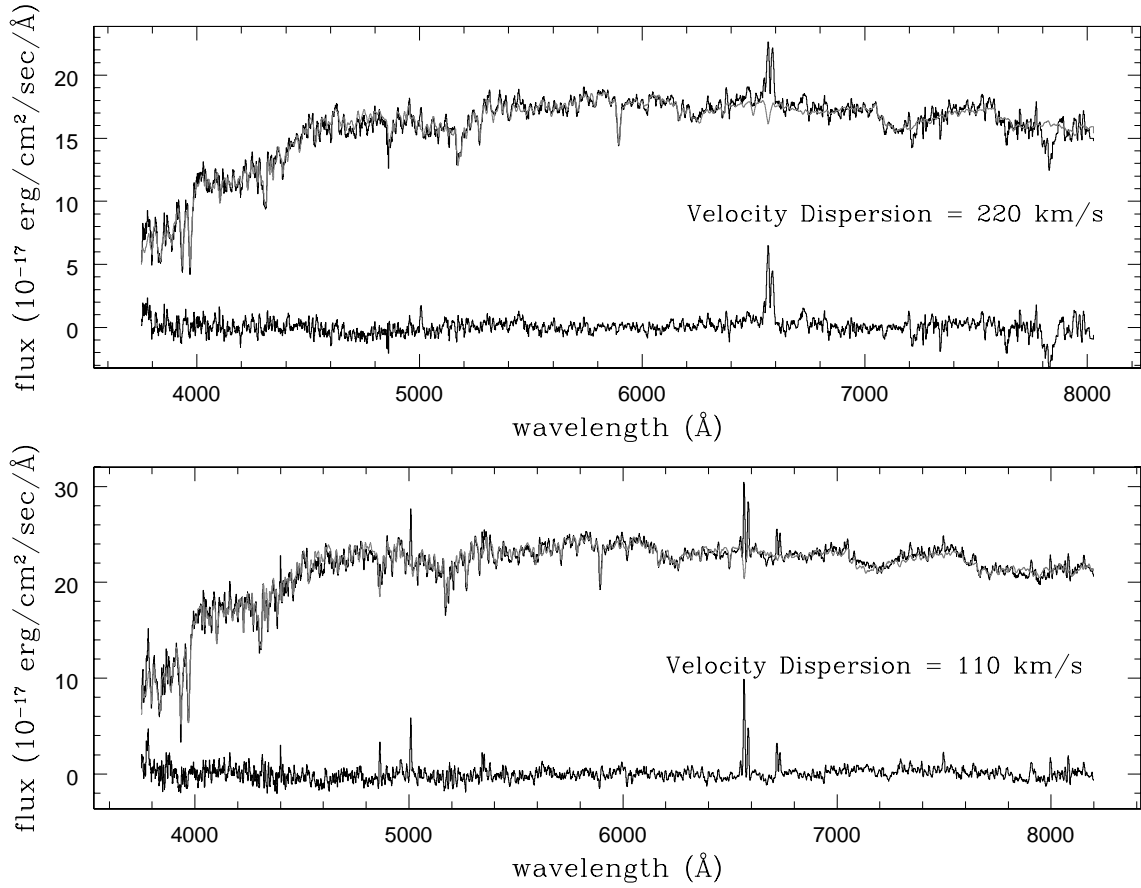


Fig. 4.— The subtraction using the same set of eigenspectra templates works well for galaxies with very different host stellar velocity dispersions. The color notation is the same as in Figure 2. Note in particular that there are no substantial residuals around the strong absorption lines in the two cases.

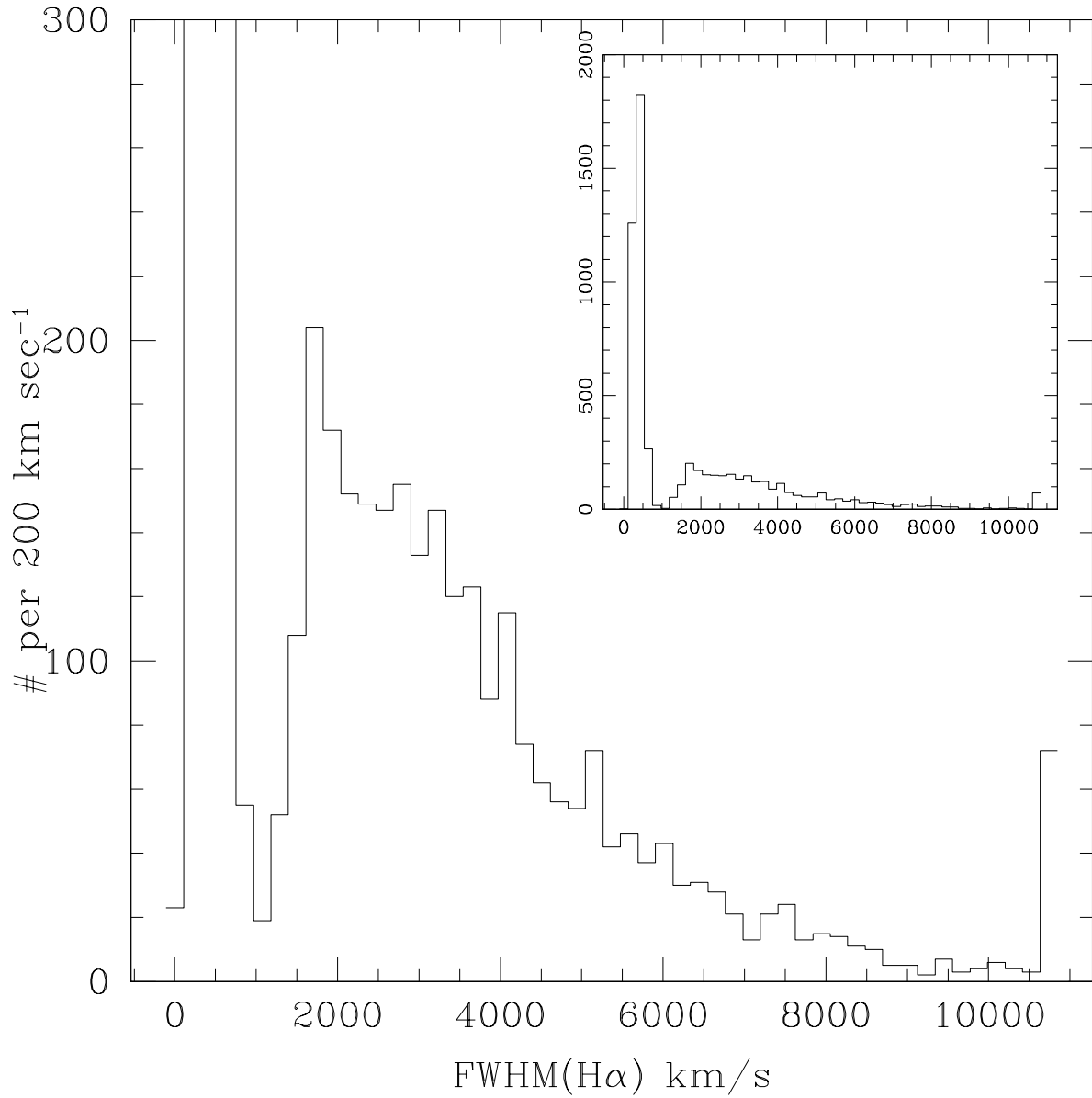


Fig. 5.— The H α FWHM distribution for emission line galaxies. The inserted plot is the H α FWHM distribution for narrow-line AGN and broad-line AGN after removing star-forming galaxies.

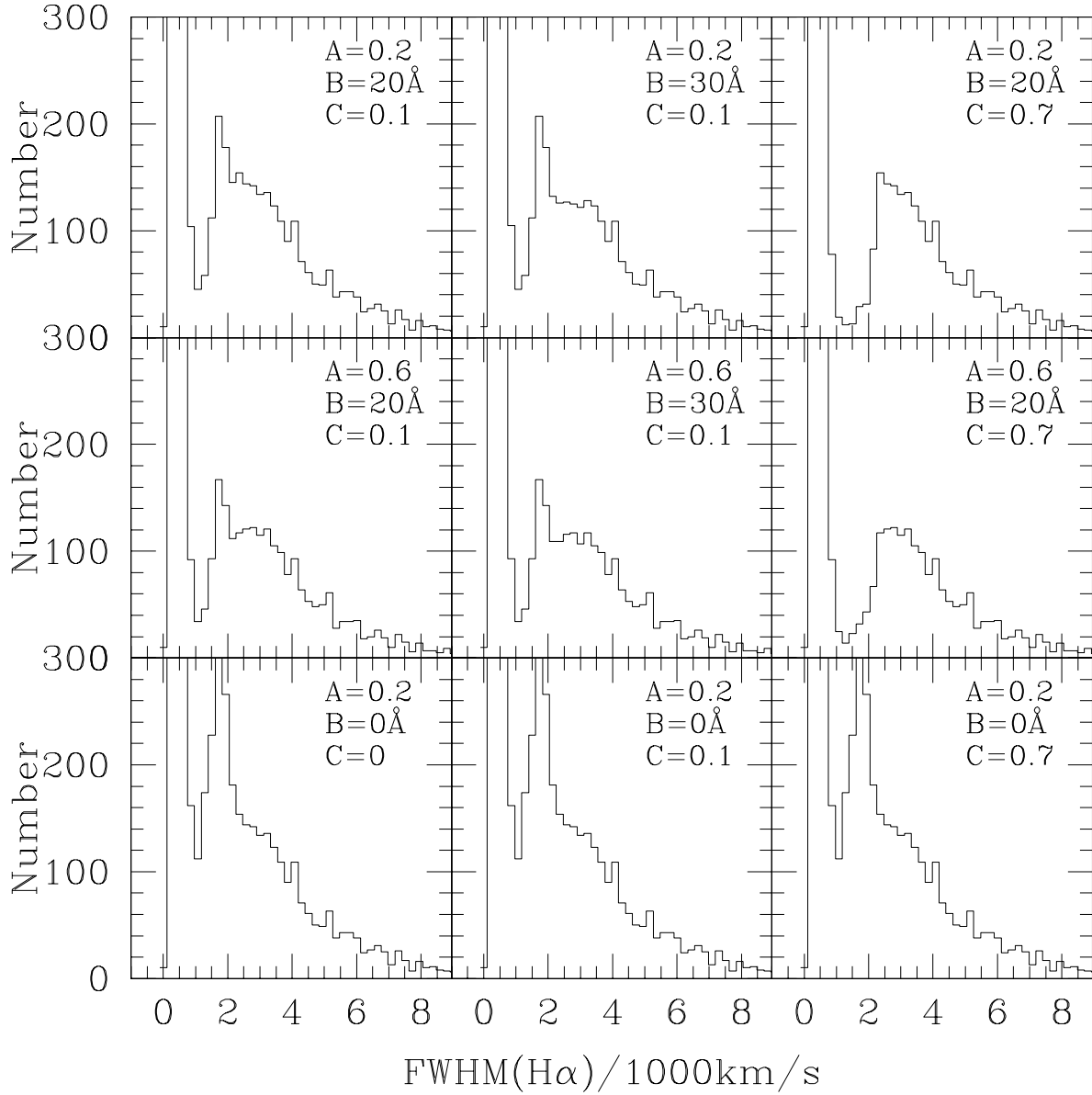


Fig. 6.— The distribution of $H\alpha$ width for emission line galaxies with various criteria (cf, equation (7)) for choosing the four-Gaussian model for the $H\alpha$ and $[NII]$ lines over the three-Gaussian model. The existence of the bimodal feature is insensitive to the exact criteria used.

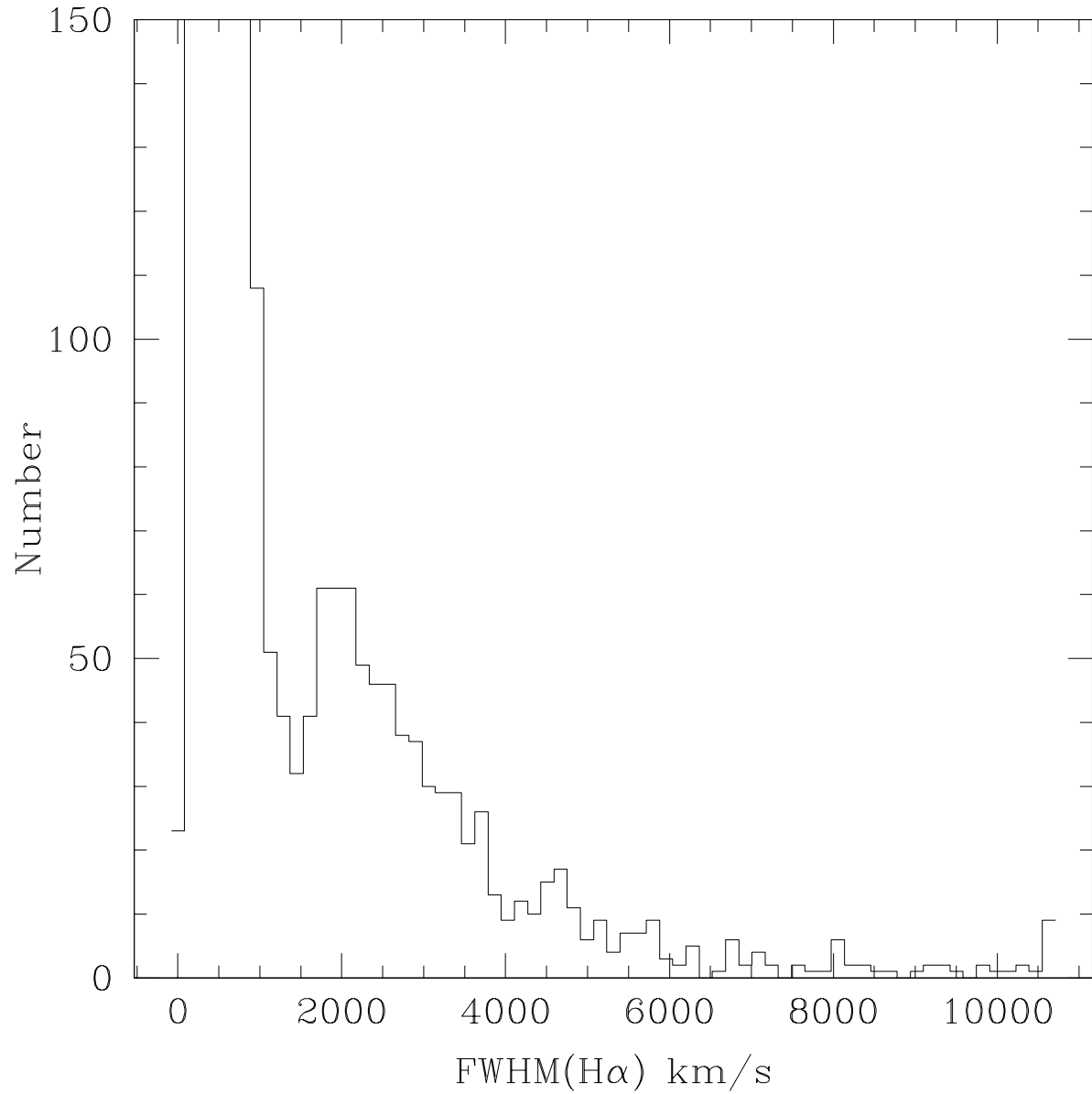


Fig. 7.— The H α FWHM distribution of emission line galaxies, when the H α and [NII] lines are fitted with a three-Gaussian model in all galaxies.

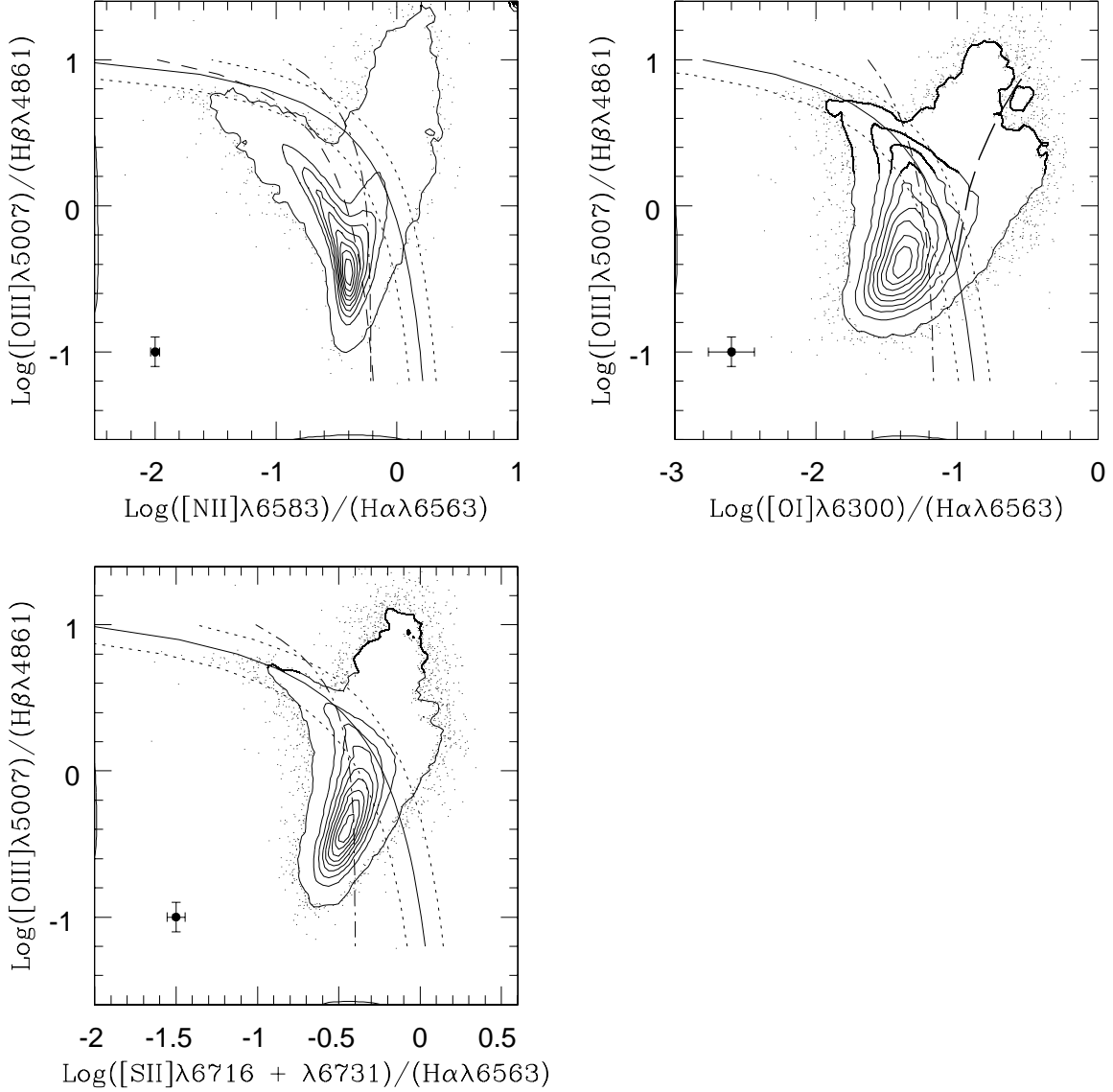


Fig. 8.— Emission-line diagnostic diagrams with the separation lines taken from Kewley et al. (2001) (solid), Kauffmann et al. (2003a) (short-dashed) and Veilleux & Osterbrock (1987) (dot-dashed). The dotted lines are the ± 0.1 dex of Kewley’s separation. The contour plots are density contours of narrow emission line galaxies with relevant emission lines detected at least 3σ significance (the typical error is shown in the lower left corner). The long-dashed line in the $[\text{OI}]/\text{H}\alpha$ vs. $[\text{OIII}]/\text{H}\beta$ diagram is the extreme mixing line (Kewley et al. 2001), to the right of which are possible AGN with very low ionizations, i.e. LINERs.

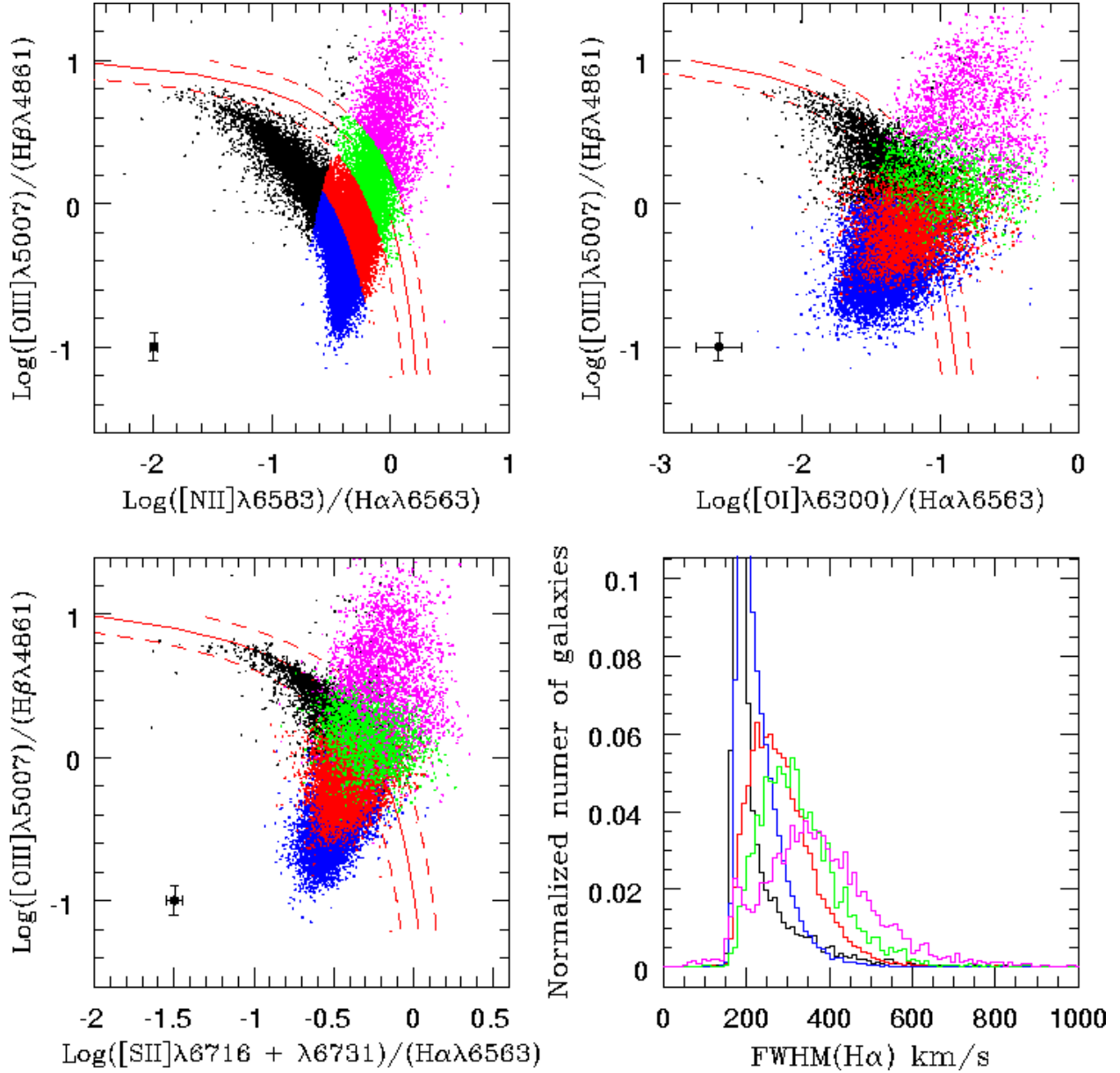


Fig. 9.— Diagnostic diagrams with Kewley’s separation lines (solid). The galaxies are colored by their locations on the [NII]/H α diagram. In the lower right figure, the distribution of H α FWHM of galaxies in each color group is plotted in the corresponding color. The typical error is shown in the lower left corner.

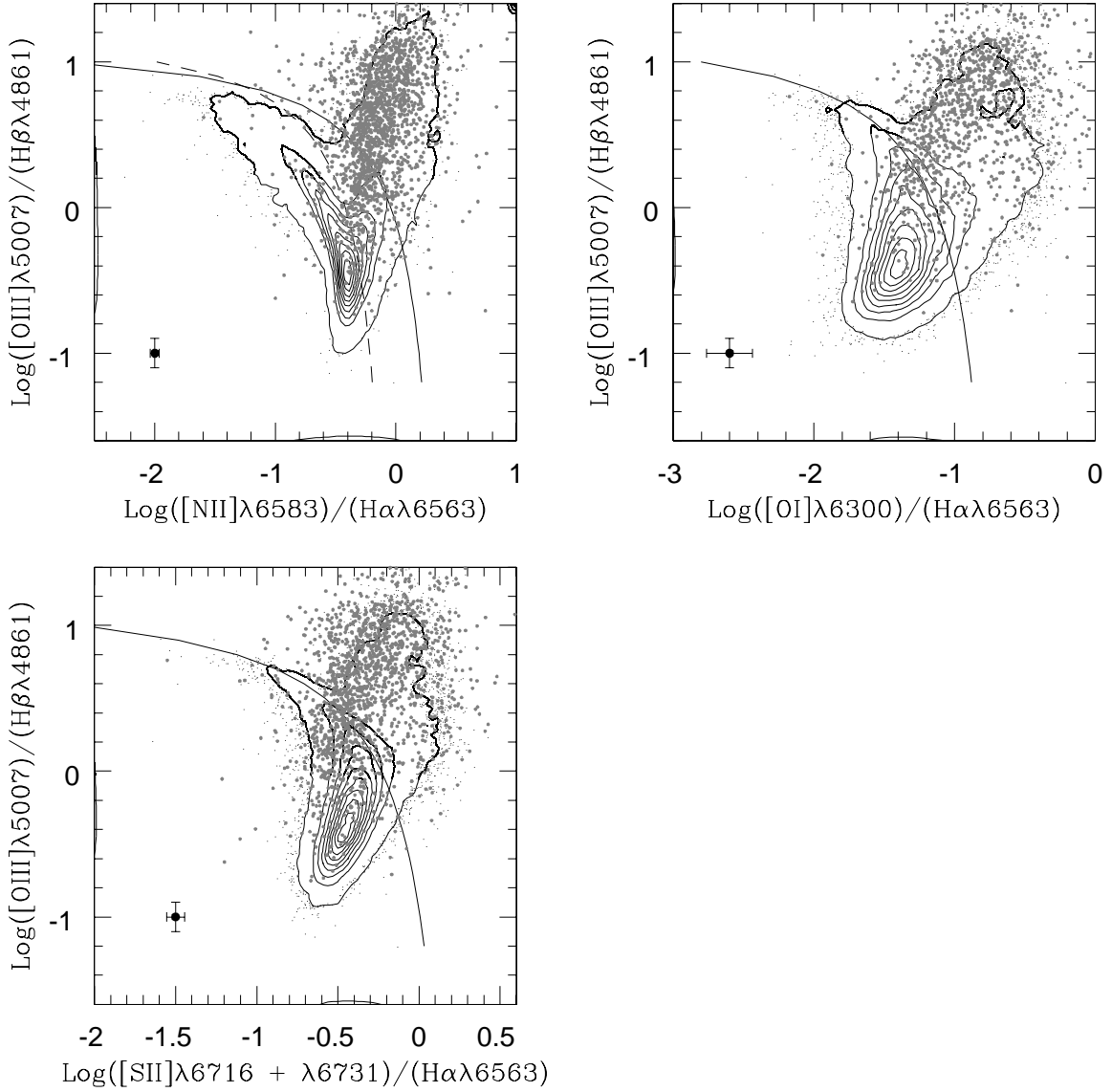


Fig. 10.— Diagnostic diagrams with large points representing the locations of narrow components of broad-line AGN. The solid lines, short dashed line and errorbars are the same as in Figure 8. Note that most points are located in the AGN region of the diagram.